



Interaction of heterogeneous and homogeneous kinetics with mass and heat transfer in catalytic reforming of logistic fuels

L. Maier^a, M. Hartmann^b, S. Tischer^a, O. Deutschmann^{a,b,*}

^a Institute for Nuclear and Energy Technology, Karlsruhe Institute of Technology (KIT), Campus North, Hermann-von-Helmholtz-Platz 1, 76344 Eggenstein-Leopoldshafen, Germany

^b Institute for Chemical Technology and Polymer Chemistry, Karlsruhe Institute of Technology (KIT), Campus South, Kaiserstraße 12, 76128 Karlsruhe, Germany

ARTICLE INFO

Article history:

Received 27 September 2010

Received in revised form 10 October 2010

Accepted 8 November 2010

Available online 7 December 2010

Keywords:

Partial oxidation

Fuel surrogates

Rhodium

Hydrogen

Catalysis

Numerical simulation

ABSTRACT

A modeling and simulation concept is presented for a better understanding of the interaction of heterogeneous and homogeneous conversion with mass and heat transfer in compact, autothermal reformers of logistic fuels for the production of hydrogen-rich synthesis gas. The model couples elementary-step based reaction mechanisms with a two-dimensional parabolic description of the flow field in a representative number of monolith channels and of heat transport in the entire solid structure of the reactor including catalyst, heat shields, insulation, and reactor wall. The concept is applied to analyze conversion, selectivity, and temperature profiles in partial oxidation of iso-octane, a gasoline surrogate, over a rhodium/alumina monolithic catalyst. The counter-intuitive flow rate effect on hydrogen yield is explained by the ratio of chemical heat release to physical heat loss. Coking tendency is related to the C/O ratio, the flow rate, and the occurrence of homogeneous fuel conversion. C/O ratios close to unity and reasonably high flow rates are found to maximize hydrogen yield at minimum production of coke precursors.

© 2010 The Combustion Institute. Published by Elsevier Inc. All rights reserved.

1. Introduction

The better understanding of the kinetics of homogeneous combustion systems and the development of elementary-step reaction mechanisms in the second half of the last century led to the detailed modeling and simulation techniques that are commonly used today to support development, design, and optimization of technical combustion systems [1–8]. In the last two decades, the progress in fundamental surface sciences and the development of diagnostic tools for studies of near-wall effects also allowed the development and, subsequently, the application of heterogeneous reaction mechanisms in modeling and simulation of catalytic combustion systems [9–15]. In both homogeneous and heterogeneous combustion the interaction of kinetics with mass and heat transfer is well-known to be essential for a reliable prediction of the combustion device's behavior. Even though turbulent flows are still not fully understood, today's models allow decent numerical simulation of the interaction of transport and chemistry in combustion devices. Significant progress has also been made in the computation of catalytic combustion

systems during the last years. In the 1990s, research focused on catalytic combustion of light hydrocarbons, in particular of natural gas, at lean conditions driven by potential gas-turbine applications [16–18] and at rich conditions driven by new routes to produce basic chemicals such as synthesis gas (CO and H₂) and olefins [19,20]. Later, special attention was given to new features of catalytic combustion in microreactor devices, in particular looking at flammability limits as well as ignition and extinction behavior, which often differ from the well-known behavior in macro-scale systems [21,22]. Even though the interaction of heterogeneous and homogeneous reactions in those devices was elucidated to be essential for conversion of C₂₊ species and at high pressures, for instance, for the understanding of the synthesis of ethylene by oxy-dehydrogenation of ethane over platinum [23,24], the chemical reaction schemes used were still rather simple, having few hundred reactions at maximum. In modeling of automobile exhaust-gas after-treatment systems with detailed reaction schemes, which has been becoming more popular in the last decade [25,26], there is little impact of homogeneous reactions on the overall conversion of the pollutants. The challenge here is rather the continuous variation of all inlet conditions and the channel-to-channel variations coupled with transient heat transfer phenomena.

Today, in the debate on alternative fuels and green-house gases, devices are discussed in which the coupling of complex homogeneous and heterogeneous chemical reaction schemes with

* Corresponding author at: Institute for Chemical Technology and Polymer Chemistry, Karlsruhe Institute of Technology (KIT), Campus South, Kaiserstraße 12, 76128 Karlsruhe, Germany. Fax: +49 721 608 4805.

E-mail address: deutschmann@kit.edu (O. Deutschmann).

heat and mass transfer matters for reactor and combustor behavior, often even superimposed by transient modifications of the active catalytic phase, e.g. by oxidation and coking. Two examples of such systems being currently of great technological interest are the solid-oxide fuel cell (SOFC) [27,28] when operated with non-pure hydrogen fuels, e.g. partially reformed logistic fuels, and short-contact time reactors for reforming gasoline and diesel fuels [29,30], for instance, as first stage of an on-board auxiliary power unit (APU). The non-linear coupling between a variety of physical and chemical processes in such chemical reactors sometimes leads to counter-intuitive experimental observations such as the increase in conversion with decreasing residence time in short-contact time reactors.

In this paper, we will present a modeling and simulation study on a catalytic reformer for the production of hydrogen-rich synthesis gas from the gasoline surrogate iso-octane. This example exhibits all features mentioned above: complex homogeneous and heterogeneous reaction schemes, mass and heat transfer effects as well as catalyst deactivation. Coupling of models of these phenomena and their computational implementation will not only be used to numerically predict the reactor behavior at varying inlet conditions such as flow rate and fuel-to-oxygen ratio but also to explain interesting reactor phenomena such as the increasing conversion with decreasing residence time.

Recently a variety of studies has been published with the focus on hydrogen production from logistic transportation fuels by catalytic partial oxidation (CPOX) [30–37]. In the last almost two decades, the pioneering work of the Schmidt group at Minnesota led to hundreds of studies, in which basically all gaseous, liquid, and solid hydrocarbon containing fuels, from natural gas to biomass, have been shown to efficiently produce synthesis gas over rhodium-based catalysts within a fraction of a second. The used so-called short-contact time reactor can be operated autothermally at temperatures above 1000 K. Short monolithic honeycomb and foam structures made out of metal oxides usually serve as catalyst carrier. Due to the high fuel throughput the reactors are nearly adiabatic; however, the small heat release is of importance for understanding the reactor behavior at varying flow rate. Compact designs can be realized due to high throughputs making CPOX reactors attractive for on-board supply of hydrogen and reformat fuel from conventional logistic as well as synthetic fuels, which can be integrated into auxiliary power units based on proton exchange membrane (PEMFC) and solid-oxide (SOFC) fuel cells [38].

Homogeneous conversion of methane in the gas phase of CPOX reactors requires high pressure and temperatures above 1200 K due to the short residence time and its low reactivity [39–41]. However, gas-phase reactions are likely for any heavier hydrocarbon fuel, even at atmospheric pressure [23,42,43]. Hence, heterogeneous and homogeneous reactions in CPOX of higher hydrocarbons are not only coupled by adsorption and desorption of fuel and oxygen molecules and their products but also by adsorption and desorption of intermediates and radicals generated either in the gas phase or on the surface. Therefore, mass transport of radicals and intermediates from/to the gaseous bulk phase and to the catalyst containing washcoat by radial diffusion in the small channels of the monolith is crucial for the interaction of heterogeneous and homogeneous reactions in CPOX reactors [44]. Furthermore, heat transfer effects become significant for the product composition [45]. Due to this complexity in chemistry and species transport, the application of detailed models for numerical simulation of CPOX reactors has only recently been extended from light hydrocarbon fuels such as methane and ethane [23,39,40,46] to liquid fuels [44,47,48]. We recently have used detailed (elementary-step) reaction mechanisms for heterogeneous and homogeneous chemical reactions as well as mass and heat transport models to study processes in a single monolith channel [44]. The formation of undesired by-products and the role of homogeneous

gas-phase reactions were discussed in the light of the formation of soot precursors through homogeneous gas-phase reactions at rich operating conditions and high temperatures.

The effects of flow rate on conversion and selectivity in CPOX reactors were studied by Krummenacher et al. with *n*-decane and *n*-hexadecane focusing on the influence of the fuel on product distribution [29]. In their paper, a beneficial effect of high flow rates on hydrogen production was noticed without prediction of a general trend due to overlapping effects of coking of fuel upstream the catalyst. In their study on CPOX of *n*-butane over supported Rh catalysts, Seyed-Reihani and Jackson found decreasing fuel conversion and a trend towards total oxidation with decreasing flow rate [49]. The experiments in non-adiabatic reactors show that for a C/O atomic ratio of 1.0 and catalyst-contact time of approximately 50 ms, improving reactor adiabaticity dramatically increases *n*-butane conversion and H₂ and CO selectivity. Rising inlet-flow temperature increases fuel conversion but does not improve H₂ selectivity. However, higher flow rates with catalyst-contact times below 40 ms show further increase in fuel conversion and synthesis gas selectivity. Beretta and Forzatti studied the CPOX of ethane and propane under isothermal operation conditions from 500 to 720 °C in an annular reactor [50]. Whereas for platinum catalysts the selected flow rate had no effect on product distribution at constant temperatures, for rhodium a notable impact was found for intermediate residence times. Aartun et al. [51] investigated temperature profiles and residence time effects during catalytic partial oxidation and oxidative steam reforming of propane in Rh impregnated metallic microchannel reactors. The experiments showed that reducing the residence time below 10 ms gave increased hydrogen and CO selectivity and reduced by-product formation, indicating suppression of the gas-phase reactions. Tavazzi et al. [52] performed the dynamic and steady-state CH₄ partial oxidation tests in a packed-bed reactor over a Rh-based catalyst supported onto Al₂O₃ spheres. The experiments at low flow rates showed that the process was governed by thermodynamics and the heat dispersion significantly affected the steady-state response of the reactor. Upon increasing the flow rate, a kinetic effect of contact time was observed. The catalytic bed progressively heated up and the adiabatic behavior was approached at the highest flow rate as a result of the predominance of the reaction enthalpy release over the heat losses. Ding et al. [53] performed CFD simulations of methane CPOX on a rhodium-coated foam monolith with detailed chemistry, revealing the effects of wall heat conduction, the channel diameter and the catalytic surface area on the profiles of temperature and species concentrations. The results showed that the maximum wall temperature, which was crucial for the catalyst stability, could be significantly reduced by increasing the thermal conductivity of the wall, and/or the channel diameter, and/or the catalytic surface area. CFD simulations combining multistep surface reaction mechanisms with a reactor model capturing heat and mass transport provide critical insight into the role of thermal processes and indicate a need for detailed mechanisms to model how competitive reaction pathways impact performance in catalytic partial oxidation reactions [54].

In a recent study [55], we also experimentally studied the impact of the mass flow rate on fuel conversion, selectivity, and operation temperature using iso-octane and a rhodium/alumina coated honeycomb monolith for a wide variety of molar carbon-to-oxygen ratios (C/O). At stoichiometric conditions (C/O = 1.0) hydrogen yields significantly increases with increasing flow rate. At lean conditions (C/O = 0.8), the measured catalyst outlet temperature was observed to increase with increasing flow rate but little impact on conversion and selectivity was observed, which could in principle be understood by a numerical simulation of heat transport in the catalytic monolith coupled with a two-dimensional flow field description of the individual monolith channels. Because the

numerical study focused on lean conditions, where homogeneous conversion is negligible, the model considered only heterogeneous reactions. Furthermore, this study indicated that the understanding of the counter-intuitive impact of mass flow on conversion at $C/O = 1.0$ requires more sophisticated numerical simulations.

The present paper does not only serve as an example to discuss the currently available methods in modeling the interaction of homogeneous and heterogeneous chemistry and mass and heat transport in catalytic combustion but also presents a significant step forward in numerical simulation of CPOX reformers operated with logistic fuels. Although more complex fuels have already been studied experimentally [47,48,56–59], data from an experimental study of a single-component reference fuel iso-octane (i-octane, 2,2,4-trimethylpentane) [55] are chosen as reference because detailed reaction mechanisms of CPOX of iso-octane over Rh have recently been developed and coupled with homogeneous reaction schemes [44]. Both mechanisms are applied in the current study without further modification. From a simulation point of view, the major novelties of the current study are: (1) the model includes the heat shields in front and beyond the catalytic section of the reactor, (2) homogeneous reactions are included in the model, (3) the impact of flow rate on yields can be explained for varying C/O ratios.

2. Experimental reference

In this present numerical study, experimental data are used as reference, which were obtained in a laboratory experiment recently set-up to study CPOX of hydrocarbons and alcohols at short-contact times under well-defined initial and boundary conditions. The reactor configuration was developed using CFD simulations of the mixing section [47] to guarantee rapid mixing of vaporized fuels with synthetic air to feed the catalyst with a homogeneous, pulse-free mixture at a uniform temperature. All relevant species present in the product stream are detected by a variety of simultaneously applied analytical methods: FT-IR, MS, and a paramagnetic gas analyzer. Combination of these techniques ensures well-closed balances for carbon, hydrogen, and oxygen and permits time-resolved monitoring of at least 12 species on the order of seconds. Further carbon containing species are detected by GC-MS, however, with much smaller time-resolution, i.e., less frequent data [44].

In Fig. 1, the heart of the reactor is illustrated. An industrially manufactured honeycomb catalyst (900 cells per square inch (cps); rhodium loading = 1.41 mg/cm^3) is used. The monolith is made out of cordierite and is 10 mm in length and 19 mm in diameter. The inner channel walls are coated with rhodium dispersed in an alumina washcoat; no further additives are used. The catalyst is positioned 200 mm downstream of the mixture inlet. Upstream and downstream of the catalyst, an uncoated foam monolith ($\gamma\text{-Al}_2\text{O}_3$, 85 pores per inch (ppi)) and an uncoated honeycomb monolith (600 cps), respectively, are placed close to the catalyst. Both non-catalytic monoliths are 10 mm in length and 19 mm in diameter and are used as heat shields and fixations for thermocouples (front face: Type K, back face: Type N). The monoliths are fixed inside the quartz tube by a quartz wool insulation tape tightly wrapped around the monoliths to avoid by-pass of gases.

The C/O ratio is used as parameter for the description of the composition of the mixture entering the catalyst; it is defined as the ratio of the total number of carbon atoms to the total number of oxygen atoms in the inlet mixture. The iso-octane/oxygen mixture diluted by 80 vol.% nitrogen is fed to the reactor at 463 K (190 °C) at total flow rates of 2, 3, 4, 5, and 6 slpm at atmospheric pressure.

For a detailed description of the experimental set-up, catalyst, analysis devices, and measurement procedures it is referred to recently published papers [44,47,56,60].

3. Modeling approach and numerical implementation

The reactor set-up ensures homogeneous mixing and avoids any gas-phase reactions upstream the catalyst. A tube-in-tube configuration leads to rapid mixing of the vaporized fuels with synthetic air to feed the catalyst with a homogeneous, pulse-free mixture at a uniform temperature [44]. Heat transfer upstream the front heat shield can be neglected because there is no significant temperature difference between inlet gas temperature and temperature of the solid entrance region of the upstream foam (Fig. 1), which exhibits a too low temperature for significant radiant heat transfer. It is likely to find some homogeneous conversion in the near downstream section of the reactor, just beyond the back heat shield, due to the still high temperature leading to slight modification of the gas-phase concentrations measured in comparison with the ones computed at the catalyst exit [48]. However, since almost all conversion and heat transfers occur within the solid structures of the reactor, i.e. catalyst plus front and back heat shields, an adequate model should consider at least these three sections. Here, we model the heat transfer in all three monoliths by a two-dimensional heat balance coupled with models for the reactive flow through a representative number of individual monolithic channels. The single-channel simulation includes detailed models for heterogeneous and homogeneous reactions.

3.1. Modeling the temperature of the solid monolithic structures

The heat of reaction of the fuel's catalytic partial oxidation is released in the catalytic section of the reactor. Some heat release due to homogeneous conversion may occur in the hot upstream part of the front heat shield's back side and, even more important, in the downstream back heat shield. Heat transfer occurs within the monolith due to conduction, mainly in the touching solid phases, as well as convection due to the gaseous flow, thermal radiation, and thermal conductivity through the thermal insulation around the monoliths inside the quartz tube, which has a severe effect on the temperature distribution. Therefore, the catalytic channels will essentially not behave alike. In particular, the outer channels will experience lower temperatures, thus lowering the overall conversion and modifying the selectivity. Therefore, the model needs to consider many channels, but usually not all channels.

Individual channels are combined into a transient temperature model for the monolithic bulk; for details it is referred to [61]. The temperature field of the monolith is treated as a homogeneous continuum in two dimensions. The evolution of the transient temperature field T can be written as:

$$\rho c_p \frac{\partial T}{\partial t} = - \frac{\partial}{\partial x_i} \Phi_{H,i} + q_H, \quad (1)$$

with ρ effective density of the monolith, c_p specific heat capacity, Φ_H heat flux vector, and q_H heat source term due to heat transfer between solid bulk and fluid flow in the channels at the gas-surface interface. The spatial coordinates, x_i , are assigned in a way that x_1 represents the axial direction of the monolith channels. The diffusive heat flux inside the monolith is modeled by anisotropic heat conduction

$$\Phi_{H,i} = - \lambda_{ij} \frac{\partial T}{\partial x_j}, \quad (2)$$

where the heat conduction coefficient λ can take different values for the axial and radial directions. The modeled reactor may consist of several layers with different material properties to account for insulation, etc. All properties are functions of temperature. Heat fluxes including terms for conduction, convection, and radiation are defined as boundary conditions. The heat source terms are calculated

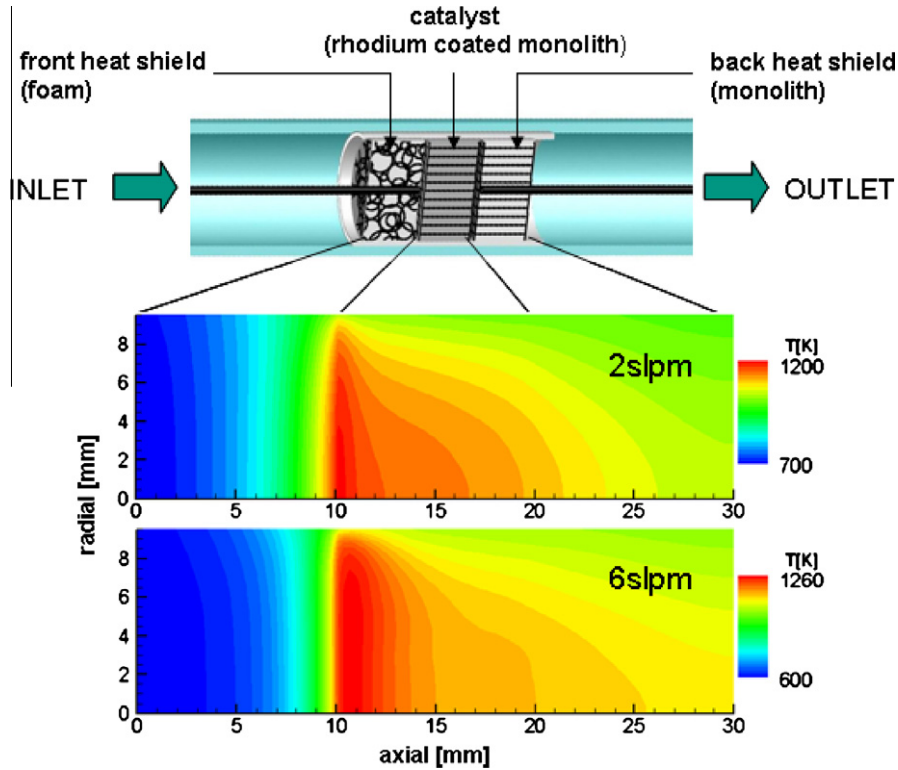


Fig. 1. Sketch of the catalyst section of experimental set-up with two heat shields simulated (top) and numerically predicted steady-state monolith temperature at $C/O = 1.0$ and at flow rates of 2 slpm (top) and 6 slpm (bottom). The symmetry axis of the monolith is at radial dimension of zero.

during the simulation of the flow through the channels as discussed below. The heat transfer from the gas phase into the solid and vice versa is indicated by a change of the integral enthalpy flux \dot{H}_{gas} in the gas phase:

$$q_H = -\sigma \frac{\partial \dot{H}_{\text{gas}}}{\partial x_1} \quad (3)$$

The channel density σ denotes the number of channels per unit area of the cross-section. Since the numerical simulation of the fluid flow is the most time consuming step, not every individual channel is simulated in detail. A representative number of channels needs to be considered only. Using a cluster algorithm, the choice of representative channels can be conducted efficiently [61]. This approach is realized in the computer code DETCHEM^{MONOLITH}, which uses the code DETCHEM^{CHANNEL} for the simulation of the individual channels [62]. The computer code automatically determines the number of channels at each time step based on a user-given tolerance, expressed as maximum temperature difference between the individual channel temperature profiles [61]. The number of channels used in the current simulation at steady-state is between eight and ten depending on the flow conditions.

A computational domain for numerical simulation is chosen according to the experimental study having a monolithic structure of 19 mm inner diameter and including the thermal insulation and quartz tube (22 mm outer diameter). In axial direction, the 10 mm front heat shield, 10 mm catalyst zone, and 10 mm back heat shield are included. Due to radial symmetry, only one half of the axial cross-section of the reactor tube is considered.

The boundary condition on external surfaces of the quartz tube include a heat-transfer coefficient of $h = 20 \text{ W}/(\text{m}^2 \text{ K})$. Since the heat-transfer coefficient can hardly be directly derived from the reactor set-up and operating conditions, the coefficient was estimated in a such way that computed and measured temperature at the catalyst outlet match. This estimation was conducted in a

former study [55] for one specific set of operating conditions, and has there as well as here been used without further modification. Temperature-dependent transport properties in the gas phase were calculated using kinetic theory; effective heat conductivities of the quartz and alumina support were chosen according to literature data [63]. The thermal conductivity and heat capacity of rhodium coated cordierite monolith were modeled as polynomial functions of temperature. The bulk density of catalyst and heat shield monoliths were measured experimentally. The material properties used in this numerical study are given in Table 1.

3.2. Flow field in the catalytic channel

The single catalytically coated channel is approximated by an axis-symmetric cylinder leading to the axial and radial spatial coordinates as independent variables. The basis of the flow field

Table 1
Material properties of the monolith used in the model.

| Physical properties | Rh coated cordierite monolith (900 cps) | Uncoated alumina foam (85 ppi) | Uncoated cordierite monolith (600 cps) | Insulation/quartz |
|--|---|--------------------------------|--|-------------------|
| <i>Heat conductivity [W/(m K)]</i> | | | | |
| Radial direction λ_{rad} | ^a | 1.1 | 1.0 | 1.36 |
| Axial direction λ_{axi} | ^b | 1.1 | 1.0 | 1.36 |
| Bulk density ρ (kg/m ³) | 540 | 976 | 283 | 2202 |
| Bulk volumetric heat capacity C_p [(kg K)] | ^c | 800 | 540 | 730 |

^a $0.2664 + 1.839 \times 10^{-4} T/\text{K} - 2.490 \times 10^{-7} T^2/\text{K}^2 + 1.720 \times 10^{-10} T^3/\text{K}^3$.

^b $0.4261 - 3.029 \times 10^{-5} T/\text{K} + 1.349 \times 10^{-7} T^2/\text{K}^2 + 3.053 \times 10^{-10} T^3/\text{K}^3$.

^c $-472 + 6.563 \times T/\text{K} - 1.120 \times 10^{-2} T^2/\text{K}^2 + 8.800 \times 10^{-6} T^3/\text{K}^3 - 2.582 \times 10^{-9} T^4/\text{K}^4$.

simulations are the Navier–Stokes equations coupled with governing equations describing the heat transport in the fluid phase and the species mass balances. Since the residence time in the monolith is on the order of milliseconds, the transport in axial direction is mainly determined by convection. Therefore, axial diffusion can be neglected, reducing the elliptical structure of the steady-state Navier–Stokes equations to a parabolic one by application of a boundary-layer approximation [8,64,65]. The resulting governing equations are a large system of parabolic partial differential equations (PDEs) with non-linear boundary conditions arising from the coupling between the gas-phase and surface processes, which are given elsewhere, e.g. [44].

At the catalytic surface, the gaseous species mass flux produced by heterogeneous chemical reactions is balanced by the mass flux of that species in the gas phase at the gas-surface interface scaled by the ratio of catalytic active to geometric surface area, which corresponds to the amount of catalyst available for surface reactions. In this work, this ratio was experimentally determined to be 15 by CO chemisorption measurements. The molar production rate of chemical species k due to catalytic reactions is

$$\dot{s}_k = \sum_{i=1}^{N_s} \nu_{ik} k_{fi} \prod_{j=1}^{K_g+K_s} c_j^{\nu_{ij}}, \quad (4)$$

which applies for gas phase ($k = 1, \dots, K_g$) and surface ($k = K_g+1, \dots, K_s$) species. K_s is the total number of adsorbed (surface) species including a vacant adsorption site species, N_s is the number of all reactions involving the catalyst; c_j are species concentrations, ν_{ik} are the stoichiometric coefficients of the reaction equations. The forward rate coefficient k_{fi} of surface reaction i is calculated by a modified Arrhenius expression:

$$k_{fi} = A_i T^{\beta_i} \exp\left(-\frac{E_{ai}}{RT}\right) \prod_{k=1}^{K_s} \theta_k^{\mu_{ki}} \exp\left(\frac{\varepsilon_{ki} \theta_k}{RT}\right), \quad (5)$$

where μ_{ji} and ε_{ji} are parameters describing an additional dependence of the rate coefficients on the surface coverage defined as $\theta_k = ck\sigma_k/\Gamma$, with Γ and σ_k being the surface site density and the number of sites occupied by adsorbed species k , respectively [8,66].

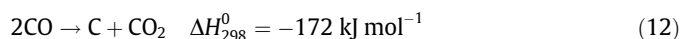
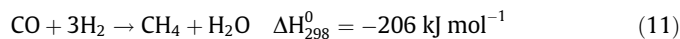
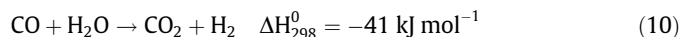
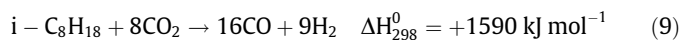
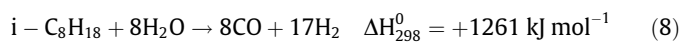
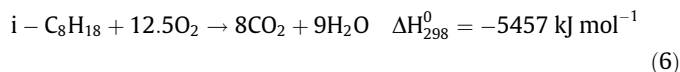
The resulting PDEs are semi-discretized by a method of lines leading to a large-scale, structured differential algebraic equation (DAE) system, which is solved using the computational code DETCHEM^{CHANNEL}; for more details, we refer to [61,62].

4. Modeling the chemistry

The reactions may not only occur on the catalytic surface but also in the gas phase due to the high operating temperatures. In particular, pyrolysis and the formation of soot precursors and soot are expected to occur in the gas-phase [44]. The only way to really understand the reaction complexity of reforming of higher hydrocarbons is the application of chemical models that are based on the molecular behavior as much as possible. Therefore, the current study applies elementary-step reaction mechanisms for modeling heterogeneous and homogeneous conversion.

4.1. Heterogeneous chemistry

Several global reactions have to be considered in partial oxidation of logistic fuels reaching from total oxidation (Eq. (6)) versus partial oxidation (Eq. (7)), steam and dry reforming (Eqs. (8) and (9)) to water gas shift reaction (Eq. (10)), methanation (Eq. (11)), carbon deposition (e.g. by the Boudouard reaction, Eq. (12)), pyrolysis (e.g. formation of ethylene), and molecular weight growth, i.e. formation of soot and soot precursors. Using iso-octane as example, those reactions can be written as:



The surface reaction model is taken from our former study [44] without any modification. This model for heterogeneous partial oxidation of iso-octane on rhodium-based catalysts uses a detailed surface reaction scheme for partial oxidation of C₁–C₃ species coupled with two additional “lumped” reactions for adsorption of iso-octane, assuming that iso-octane adsorption quickly leads to the species that are explicitly described by the detailed part of our mechanism. The detailed surface reaction mechanism consists of 56 reactions among 9 gas-phase and 17 surface adsorbed species. The detailed mechanism coupled with the lumped reactions describes all global reactions (Eqs. (6)–(12)) via a complex reaction network except olefin production and soot formation, which are unlikely to occur heterogeneously. The mechanism includes steps that can lead to a monolayer of carbon but no carbon growth mechanism is included.

4.2. Homogeneous chemistry

Several chemical reaction mechanisms are described in literature to model long chain hydrocarbon oxidation. In this study, we focus on oxidation of iso-octane serving as surrogate for gasoline fuel. The mechanisms given in literature were often developed and evaluated especially for typical homogeneous charge compression ignition (HCCI) conditions and can be divided in three groups in the order of decreasing complexity and increasing level of empiricism incorporated into the model.

4.2.1. Detailed mechanisms

In order to predict the reaction rates for all operating conditions and to analyze critical reaction pathways, the use of large, detailed mechanisms is recommended. Examples are the *LLNL mechanism* developed by Curran et al. [67] consisting of 3606 reactions among 857 species and the *Nancy mechanism* of Glaude et al. [68] consisting of 1832 reactions among 367 species.

4.2.2. Skeletal (semi-reduced) mechanisms

Using rate analysis, sensitivity analysis, and the Computer Singular Perturbation (CSP) method, a detailed mechanism can be reduced to skeletal one. For instance, the *LLNL mechanism* for iso-octane was reduced to a mechanism consisting of 258 species only by Chen et al. [69], which was used for prediction of the ignition time and CO and HC emissions over a wide range of HCCI conditions. A reaction mechanism proposed by Golovitchev et al. [70] for the oxidation of *n*-heptane and iso-octane can also be considered to belong to this methodological category. This mechanism includes 130 species and 690 reactions. Another example is the lumped kinetics model of Ranzi et al. [71] involving only a limited number of intermediate steps (145 species and 2500 reactions), which was also constructed from detailed mechanisms.

4.2.3. Reduced mechanisms

Reduced mechanisms can be generated including additional generalizing procedures and empirical rules. The species with similar functionality are combined and treated as a single entity. The reduced chemical kinetics model for *n*-heptane/iso-octane mixtures developed by Tanaka et al. [72] includes 32 species and 55 reactions and reproduces the pressure curves obtained in Rapid Compression Machine (RCM) experiments over a wide range of conditions remarkably well for an empirically based model. The mechanism is very sensitive to the fuel structure, the mixture composition, and the initial temperature and pressure. A skeletal mechanism for *n*-heptane/iso-octane mixtures containing 75 species was reduced to 19 species by Lovas et al. [73] and is able to predict ignition behavior. Much severely reduced empirically based models are available as well such as the *Shell model* based upon the low and intermediate temperature chemistry and used for simulation of hydrocarbon auto-ignition; it consists of only five species and eight reactions [74].

Obviously, the computation is far less expensive when using a reduced mechanism. However, a reduced model may provide only very limited information on the production of minor species. One may argue that in the catalytic reactor studied here, most of the conversion occurs on the surface, and therefore the implementation of a detailed, computationally very expensive mechanism is not justified by the benefits. However, some of the main technological hurdles in the application of CPOX reactors may not be understood with reduced mechanisms. These challenges are the formation of coke layers on the catalyst and soot precursor in the gas-phase. In our previous work on the impact of gas-phase reactions on post-catalytic conversion in CPOX reactors using single-channel simulations [48], we have tested two detailed schemes of Curran et al. [67] and Dean et al. [75]. Both mechanisms represent most experimentally observed trends well. However, due to the very large computational time, these detailed models cannot be used for transient simulations of entire monolithic structures, in which the number of individual channel simulations is on the order of at least 10^3 . Although, a new numerical approach [76,77] speeds up the simulation of complex (in chemistry) 2d reactive flows, the typical CPU time for a simulation with the detailed LLNL mechanism still can take several CPU hours (one processor).

On the other side, we still want to cover as many details as possible. Therefore, skeletal mechanisms seem to be the model of choice for our purpose, a reasonable trade-off between accuracy and CPU time. The skeletal kinetics reaction mechanism developed by Golovitchev et al. [70] was used in this paper to simulate the catalytic partial oxidation of iso-octane. This mechanism was able to accurately predict the ignition delays and oxidation rates for iso-octane mixtures over wide ranges of temperature and pressure and was also successfully used for computational studies of direct injection gasoline [78,79] and diesel engines [78,79] using three-dimensional computational fluid dynamics.

5. Results and discussion

Technical reformers for the production of hydrogen-rich synthesis gas by partial oxidation of logistic fuels will be operated at lean conditions regarding synthesis gas formation, which implies according to Eq. (8) molar C/O ratios below 1.0. For C/O ratios above unity, and even below unity for certain fuel components and flow rates, several recent studies revealed the production of significant amounts of coke precursors, in particular ethylene and propylene [29,44,55,56]. Hydrogen yields have been shown to exhibit a maximum of nearly 0.95 around C/O = 1.0 and high flow rates for CPOX of iso-octane and most logistic fuels over Rh cata-

lysts. Consequently, the reactor should be operated at C/O ratios as high as possible to maximize hydrogen yields but as low as possible to minimize the formation of coke precursors.

A further restriction on operation conditions is temperature; high temperatures favor hydrogen selectivity but may destroy the catalyst and even boost gas-phase reactions leading to formation of coke precursors. Since the advantage of the use of CPOX for reforming fuels is the potential to operate the reactor autothermally, the operating temperature cannot serve as a free parameter; it rather depends on conversion, selectivity, inlet gas temperature, and heat loss. In the experimental reference [55], the catalyst exit temperature measured was as high as 1420 K (1150 °C) for C/O = 0.8 and the highest flow rate tested was 6 slpm. With increasing C/O, the dependence of the catalyst exit temperature on flow rate decreases to 10 K around C/O = 1.05, and the catalyst outlet temperature falls to 1120 K (850 °C).

Consequently, the technically attractive range for the C/O ratio seems to be 0.8–1.0. It should be noted that the final optimization of the C/O ratio also needs to account for the specific fuel composition, recycling of exhaust gas, preheating of the mixture, and potential heat exchange effects by the actual technical realization of the reformer. In the remainder of this paper, we will therefore focus on the two limits of this range of conditions, C/O = 0.8 and C/O = 1.0. Concerning the dependence of the reactor behavior on the flow rate, similar hydrogen yields but different catalyst exit temperatures were observed at C/O = 0.8 and vice versa at C/O = 1.0.

5.1. Temperature and species profiles within the reactor

The numerical simulation predicts the two-dimensional temperature profile of the three monoliths of the reactor as function of axial and radial position as shown in Fig. 1 for the lowest (2 slpm) and highest (6 slpm) flow rate studied. At both conditions, the hottest zone of the catalytic (middle) monolith is in its entrance region.

Upstream heat transfer leads to a significant temperature increase of the downstream section of the front heat shield, which increases with decreasing flow rate. The residence time of the reactants within this uncoated monolith however is too small to initiate any fuel conversion in the gas-phase as clearly shown in Fig. 2. The solid temperature at the entrance of the front heat shield is already notably higher than the temperature of the incoming gas being 463 K. Depending on the flow rate the solid temperature at the entrance decreases from 660 K to 570 K for increasing flow rate from 2 to 6 slpm due to the increasing convective cooling effect of the incoming gas at C/O = 1.0 (Fig. 3b). Convective cooling has a much stronger impact on the front temperature of the front heat shield than upstream heat conduction, because the maximum temperature of the catalytic monolith is highest at 6 slpm but the front temperature exhibits the lowest value at this condition (Fig. 3b). The radial temperature distribution in the front heat shield is rather flat. Interestingly, the temperature slightly increases towards the reactor wall showing the impact of heat conduction in the dense insulation and in the quartz tube.

Within the catalytic monolith radial and axial temperature variations can clearly be seen. The monolith is cooled by heat loss at the reactor insulation and quartz tube; the effect is stronger at low flow rates, because the total amount of heat released by chemical conversion is small and the maximum temperature does not change significantly with flow rate at C/O = 1.0. Even though the temperature exhibits a stronger dependence on flow rate at C/O = 0.8, the same effect was observed [55] showing that the flow rate strongly determines the temperature profile and also the chemical conversion via the ratio of absolute chemical heat release to absolute physical heat loss.

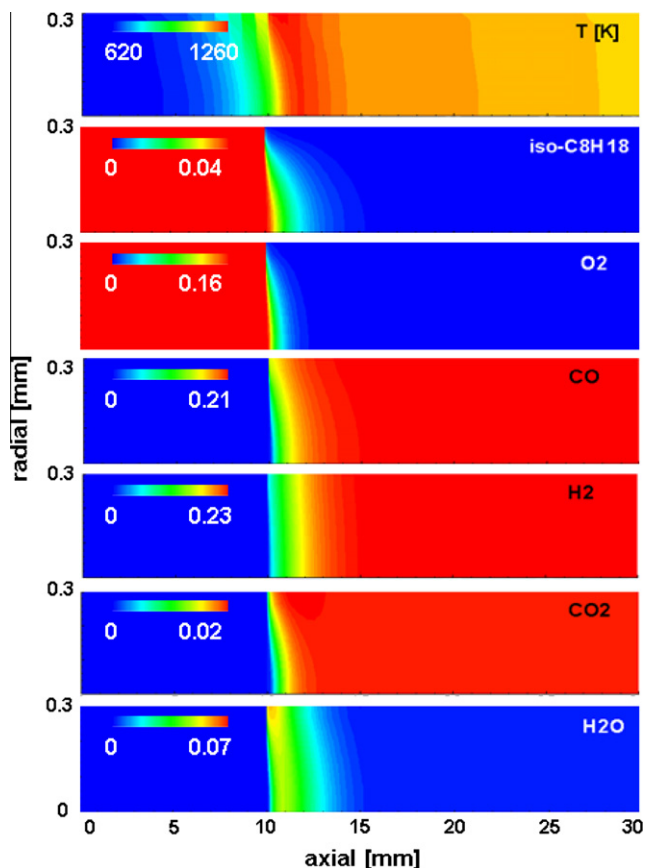


Fig. 2. Numerically predicted gas-phase temperature and mole fractions of iso-octane, O_2 , CO , H_2 , CO_2 , and H_2O in the catalytic channel at $C/O = 1.0$ and 5 slpm. The symmetry axis of the channel and the gas–wall interface are at radial position of 0 and 0.3 mm, respectively.

In axial direction, the temperature decreases rather quickly within the catalytic section after reaching its maximum at the entrance region. This behavior is well-known in CPOX reactors for all hydrocarbons studied, from natural gas to diesel, and has extensively been described in literature. To make it short (Fig. 2): in the entrance region of the catalytic monolith total oxidation of the fuel towards CO_2 and H_2O occurs until oxygen is almost completely consumed, at least on the catalyst, leading to the temperature maximum. Further downstream, steam reforming of the remaining fuel leads to the high hydrogen yields. At stoichiometric conditions ($C/O = 1.0$) not only the oxygen but also the fuel is completely (>98%) consumed within the catalytic monoliths both at low (2 slpm) and high (6 slpm) flow rates. CO is already partially

produced in the total-oxidation zone, dry reforming with CO_2 is not significant. Within few milliseconds in time or millimeters in space catalytic reforming of the fuel iso-octane is basically completed. However, the consequences of a small remaining amount of reactants is important for technical applications, such as those discussed below.

Since steam reforming is endothermic and the total heat consumption by this process depends on the total amount of fuel reformed, the temperature decreases faster for higher flow rates in axial direction in the centerline of the catalytic monolith; compare the 2 slpm versus 6 slpm case in Figs. 1 and 3b. However, closer to the wall of the reactor, the larger heat loss effect at slower flow rates exceeds the smaller (2 slpm versus 6 slpm) chemical heat consumption effect and leads to more rapid cooling in axial direction at low flow rates. Increasing flow rates lead to larger temperature gradients in axial direction and smaller ones in radial direction.

In the downstream back heat shield, the cooling effect of the surroundings also explains the more rapid cooling for lower flow rates. As shown in Fig. 3b, the axial temperature profiles of varying flow rates in the centerline of the reactor cross each other just before entering the catalyst and again around axial center of the catalytic monolith. The highest temperature maximum is obtained at the highest flow rate studied, which is even much more pronounced at $C/O = 0.8$ (not shown). On the scale used in Figs. 2 and 3a, no variation of reactants' concentration (vanished) and any major products' concentration can be recognized. From a former study, however, we know that post-catalytic reactions in the gas-phase may also lead to significant (few percent) variations of the major products' concentrations, depending on the time needed for thermal quenching of the product stream [48].

The peak temperature in a near-reactor-wall and a centerline catalytic channel may differ by as much as 100 K as shown in Fig. 3a. Consequently, the conversion, selectivity and also spatial profiles will differ. Hence, it may be risky to derive the product composition of the entire monolith based on a single-channel simulation, even though the qualitative picture will not change [44,55]. It should be noted that the equilibrium composition for $H_2/H_2O/CO/CO_2$ mixtures changes quite significantly in this temperature range of around 1000 K.

5.2. Heat balance model and flow rate dependence of the reactor behavior

The right choice of the model to account for heat transfer in CPOX reactors matters to understand the impact of the flow rate on conversion and selectivity. In our recent study [55], we discussed the impact of the flow rate on the reactor behavior in CPOX of iso-octane over Rh for $C/O = 0.8$. Using the same modeling

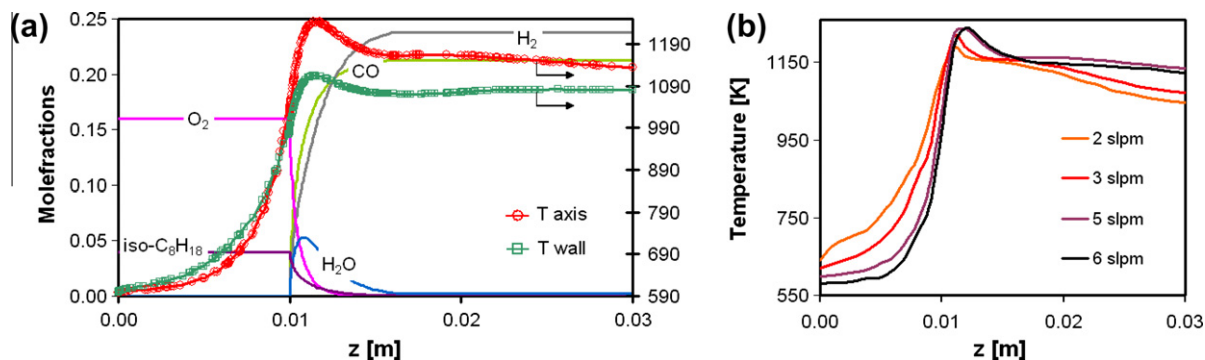


Fig. 3. Numerically predicted axial species profiles (in the center of the single channel) in the centerline of the monolith and temperature profiles in the centerline (axis) and at the outer wall of the monoliths, $C/O = 1.0$, 5 slpm (a); effect of flow rate on temperature profile taking in the centerline of monoliths, $C/O = 1.0$ (b).

approach as presented here, the catalytic section of the reactor only was simulated with two different heat transfer assumptions. The first, adiabatic model applies a single-channel simulation with adiabatic boundary conditions; in this case a single-channel simulation is sufficient. In the second model, the catalytic monolith with several representative channels was simulated including heat losses at all monolith boundaries. The inlet temperature was taken from the experiment, measured slightly upstream the interface between the front foam and the catalytic monolith. The adiabatic model was not able to predict even the qualitative behavior, i.e., the increase of the catalytic exit temperature with increasing flow rate; at $C/O = 0.8$ the hydrogen yields did not depend on flow rate. The current paper continues this study; we now simulate all three monoliths, include homogeneous chemistry, and vary the C/O ratio; the model of this paper will be called *complex model* in the remainder of this section.

Figure 4 compares the numerically predicted temperature at the outlet of the catalytic section of the reactors with the experimentally measured temperature as function of flow rate. In addition, numerically predicted outlet temperatures of a single-channel simulation with adiabatic boundary conditions are shown. The exit temperature increase with increasing flow rate is well-computed with the accurate heat balance model, while the adiabatic model fails. The increase in temperature with increasing flow rate observed in this study can be understood by the effect of heat losses. The total amount of heat released by the reaction almost linearly increases with flow rate, because fuel is fully converted in the first zone of the catalyst. The adiabatic behavior is approached at the highest flow rate as a result of predominance of chemical heat release to thermal heat loss. This relation between the absolute heat loss and the absolute chemical heat release has been discussed in our previous work [55]. It should be noted that the extensions of the complex model (three monoliths, homogeneous chemistry) in the current paper were not decisive for the qualitative understanding of this phenomenon.

At $C/O = 1$, the catalyst outlet temperature measured revealed only a slight but notable increase with increasing flow rate [55], from 1120 to 1160 K for 2–6 slpm, respectively. The simple adiabatic single channel model and the complex model were also used to understand the impact of the flow rate on temperature and species profiles at $C/O = 1$. As shown in Fig. 5, the adiabatic model is not able to reproduce the experimentally observed increase of the catalyst outlet temperature as function of flow rate, while the complex model predicts this observation even quantitatively very well. Here it should be noted that all simulations with the complex model for all C/O ratios and flow rates simulated use exactly the same parameters, i.e., not even a single chemical and physical parameter was adapted, neither in the heterogeneous and homogeneous reaction schemes, nor the catalyst site density and the

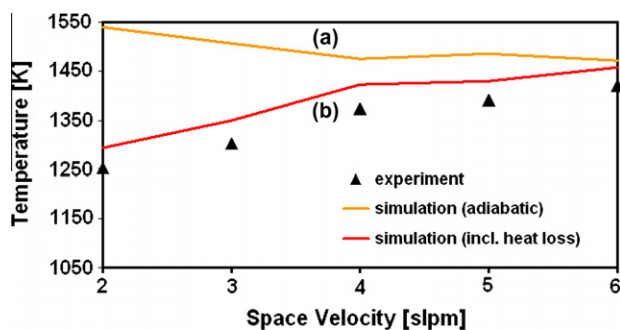


Fig. 4. Catalyst outlet temperature as function of space velocity at a given $C/O = 0.8$; experimental data versus simulation, (a) adiabatic single-channel simulation without heat loss, (b) monolith simulation including heat loss.

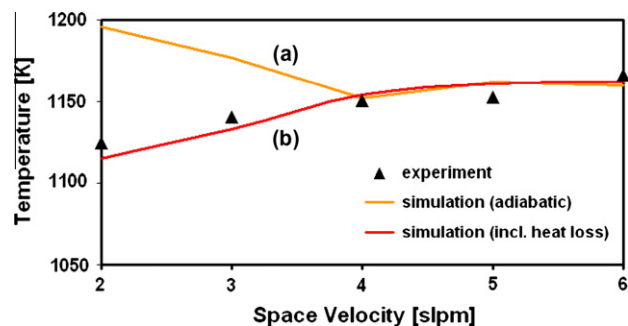


Fig. 5. Catalyst outlet temperature as function of space velocity at a given $C/O = 1.0$; experimental data versus simulation, (a) adiabatic single-channel simulation without heat loss, (b) monolith simulation including heat losses.

specific catalytic surface, nor in the heat balance's boundary conditions such as heat conductivity, thermal emissivity. Furthermore, it should also be noted that a simulation of the catalyst section only using the monolith model is not able to predict the experimental trend within this small temperature range; here the heat transfer effects between all three monoliths have to be taken into account.

The experimentally determined independence of the hydrogen selectivity on the flow rate at $C/O = 0.8$ is well-reproduced by the numerical simulation using the complex model as shown in Fig. 6a, the deviations are within the experimental error [55]. At $C/O = 1.0$ shown in Fig. 6b, the hydrogen selectivity significantly increases with flow rate up to 4 slpm and is rather constant at higher flow rates, though the temperature increases only slightly (Fig. 5). A variety of effects (heat balances, thermodynamics, kinetics, flow rate/residence time) overlap to produce this levelling-out of the hydrogen selectivity between 3 and 4 slpm. First consider the effect of residence time/kinetics: As discussed above and shown in Figs. 2 and 3, hydrogen production is mainly due to steam reforming of remaining fuel after full consumption of oxygen. The time, or better the axial catalyst distance needed to complete this reforming step, is approximately 5 mm at 5 slpm. Lowering the flow rate, i.e. increasing the residence time, should promote hydrogen production. Since just the opposite is observed, a direct residence time effect via kinetics can be excluded. Second, higher flow rates have an impact on the ratio of chemical heat release to physical heat loss to the ambient. Most of the heat release occurs in the entrance region of the catalyst, i.e. in the total-oxidation zone, leading to a temperature peak: the higher the flow rate the higher the peak temperature. Even though the position of the temperature peak slightly shifts downstream with flow rate (Fig. 3b), total oxidation is always well within the catalytic section of the reactor unless extremely high flow rates are considered [80]. Higher temperatures do not only shift the thermodynamic equilibrium towards hydrogen production but also increase the reaction rate of the second global reaction step, i.e., hydrogen production by steam reforming. In Fig. 3b it can be recognized that the negative temperature gradient in the steam reforming zone is larger for higher flow rates even though the cooling effect by heat loss of the catalyst to the ambient is smaller for high flow rates. However, the heat loss effect clearly overlaps with the flow rate effect as shown in Figs. 1 and 3b. More exterior channels of the monolith experience much lower temperatures at slow than at high flow rates and, consequently, hydrogen production is reduced. In addition to steam reforming, also the exothermic water-gas-shift reaction (Eq. (10)) leads to hydrogen production; this effect is rather small but still has some little impact on the final product composition and catalyst outlet temperature [55]. Summarizing, the understanding of the dependence of hydrogen selectivity on flow rate can only be achieved by taking mass and heat transfer as well as detailed kinetic schemes (reaction pathways) into account.

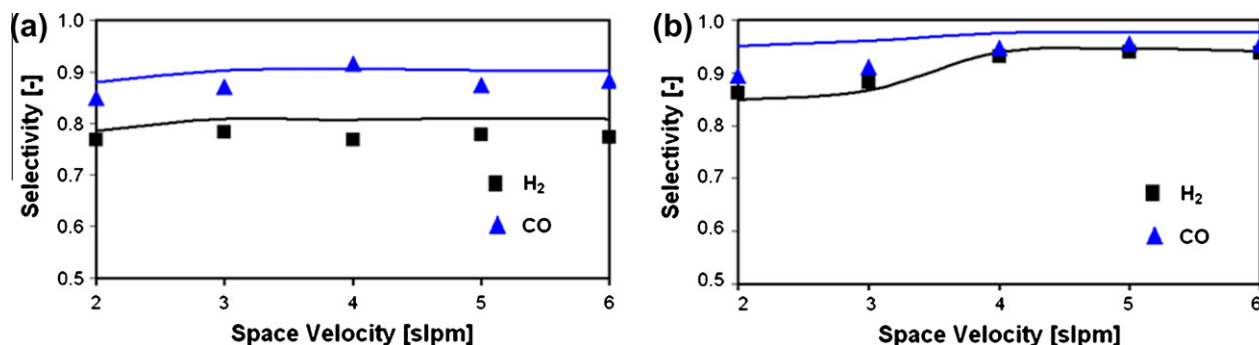


Fig. 6. H₂ and CO selectivity as function of space velocity at C/O = 0.8 (a) and C/O = 1.0 (b); experimental data (symbols) versus simulation (lines).

There definitely is a trade-off between the benefits and drawbacks of high temperatures. In autothermal operation, higher temperatures are achieved by increased total oxidation rates and decreased physical heat loss. However, because the water-gas-shift reaction is rather slow at the time scales considered here, most of the fuel that is consumed for total oxidation cannot be used for hydrogen production. Furthermore, higher catalyst temperatures also increase heat loss to the ambience and may cause degradation of the materials used. Following the discussion up to now, this modeling study may suggest C/O ratios around 1.0 and reasonable high flow rates being the optimum operational conditions. However, another potential problem has to be considered before choosing the optimum reactor conditions, the probability of the formation of coke precursors.

5.3. Impact of flow rate on gas-phase reactions

The experimental reference study [55] reveals full (100%) fuel consumption at C/O = 0.8 for all flow rates, while at flow rates below 4 slpm not all the fuel is converted at C/O > 0.9. Since it is very likely that some of the remaining fuel can still be converted in the hot section of the back heat shield or even downstream by gas-phase reactions [48], there might still be some fuel left at lower C/O ratios and/or flow rates at the outlet of the catalyst, which is a source for the formation of coke precursors [44]. We will now consider conditions, at which no remaining fuel was found, by analyzing the composition downstream the reactor, e.g. C/O = 1.0 and 5 slpm.

In Fig. 7, the profiles of several minor species are shown as computed over all three monoliths at C/O = 1.0 and 5 slpm, conditions being optimal for hydrogen production. The molar fraction of any species does not exceed 0.1%. In the simulation, all these species

are exclusively formed by gas-phase reactions, because they are either not part of the catalytic reaction model [44] or not produced in simulation without the homogeneous reaction scheme. Significant amounts of these *gas-phase chemistry* species are neither produced inside the front heat shield nor in the first catalytic zone where oxygen is still available.

A reaction flow analysis (Fig. 8) of the gas-phase chemistry model was carried out at rather rich conditions (C/O = 1.4), temperature, and residence time typically for the downstream section of the catalytic monolith. CH₃ is one of the radicals promoting pyrolysis of the remaining fuel, and iso-C₄H₈ is one of the crucial intermediates, both are primarily produced 2 mm downstream the catalyst entrance where oxygen is already fully consumed but the fuel iso-octane is still available. The radial gradients of both CH₃ and iso-C₄H₈ correspond to the radial gradients of the remaining fuel (Fig. 2); all species have a maximum at the centerline of the channel. In the same region (Fig. 7), the formation of propylene starts, a direct product of pyrolysis of iso-octane. Subsequently, propylene is converted to ethylene. The amount of benzene formed in the monolithic sections of the reactor is almost negligible. Although the concentrations of both the major coke precursors, ethylene and propylene, do not exceed 100 ppm, these amounts may be large enough to slowly but continuously form carbonaceous over-layers on the monolith channels and reactor walls and even provide a significant source for molecular growth of gas-phase particles that may harm downstream devices such as fuel cells.

Lower flow rates for C/O ~ 1.0 do not only decrease hydrogen yields but also significantly favor the formation of coke precursors as shown in Fig. 9. The formation of both ethylene and propylene increases with decreasing flow rate. The simulations predict this trend well. For flow rates of 4 slpm and above, neither ethylene

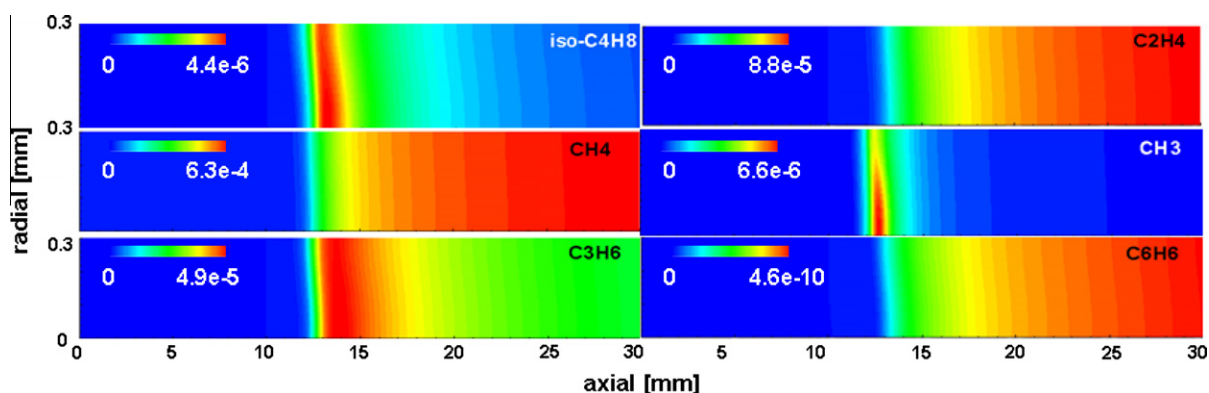


Fig. 7. Numerically predicted molar fractions of iso-C₄H₈, CH₄, C₃H₆, C₂H₄, CH₃, and C₆H₆ in all three monoliths at C/O = 1.0 and 5 slpm. The symmetry axis of the channel and the gas-wall interface are at $r = 0$ and 0.3 mm, respectively. Flow direction is from left to right.

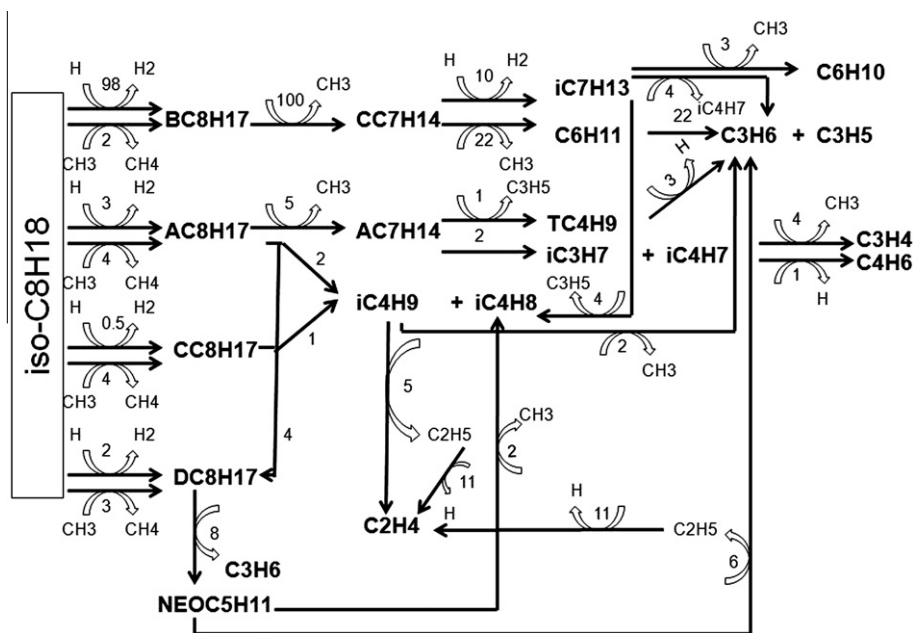


Fig. 8. Reaction rate flow analysis for pyrolysis of iso-octane at $C/O = 1.4$, 1009.7 K and after residence time of 0.042 s. The time-integrated values given are scaled in a way that the maximum molar reaction rate of an individual reaction is set to be 100. Note that only major paths are shown. Species nomenclature is given in [Suppl. Mat.](#)

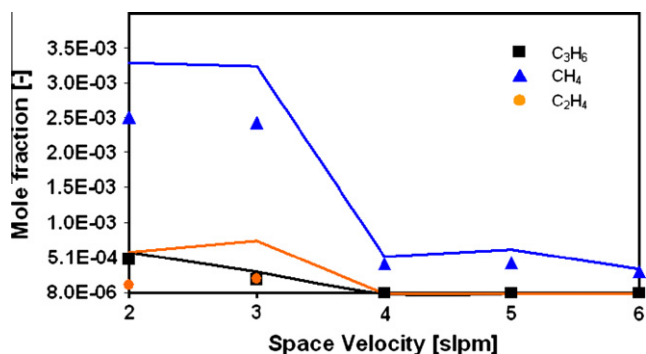


Fig. 9. Mole fraction of methane, ethylene, and propylene in the gas phase at the back face of downstream heat shield as function of space velocity at a given $C/O = 1.0$; experimental data (symbols) versus simulation (lines).

nor propylene is observed and predicted. The quantitative differences between simulation and experimentally derived concentrations may have several reasons. First of all, reactions are very likely to occur downstream the monoliths [48], which is not included in the model. Second, the gas-phase mechanism applied is a reduced one and not really established for the pyrolysis-like conditions dominant in the downstream section of the CPOX reactor. Third, the axial position at which a carbonaceous over-layer is formed on the catalytic channel wall as discussed below is difficult to predict accurately.

In order to get an impression of the influence of the chosen gas-phase reaction mechanism on the results discussed, a straightforward comparative study of the four detailed mechanisms referenced in Section 4.2 and the skeletal mechanism (Golovitchev) was conducted for varying C/O ratios. To keep the computations tractable, a simple one-dimensional flow problem without any heat and radial mass transport models was solved within the monolithic section of the reactor using the measured outlet catalyst temperature (varying with C/O) as constant reference temperature. [Figure 10](#) reveals that all five models are able to reproduce the measured

trends for both formation of propylene and methane. Taking the severe simplifications of the isothermal 1d model into account, even the quantitative numbers of the numerically predicted concentrations agree reasonably well. Due to model simplification, it does not make sense to evaluate the applicability of the individual detailed gas-phase reaction schemes for CPOX of iso-octane using the results shown in [Fig. 10](#). In the case of a flow rate of 4 slpm shown here, propylene is produced at $C/O > 1.0$ only; however, it should be noted that production of the coke precursors ethylene and propylene becomes already significant at $C/O < 1.0$ for a flow rate of 2 slpm [55].

Methane is the largest minor species produced in the CPOX reactor reaching a yield of 1.3% at $C/O = 1.0$ and 2 slpm. At higher flow rates and smaller C/O ratios the formation of CH_4 significantly decreases. In [Fig. 9](#), methane concentration falls almost by one order of magnitude between 3 and 4 slpm ($C/O = 1.0$), well-predicted by the model. Methane can be produced by gas-phase reactions and surface reactions, and actually the methane detected seems to arise from both processes. As shown in [Fig. 10](#), methane is significantly produced in the gas-phase. Analyzing the methane profile in [Fig. 7](#), methane formation starts relatively early in the reactor in a region, in which all the oxygen is consumed but the number of carbon atoms present on the catalyst surface increases without yet coking-up the catalyst ([Fig. 11](#) and discussion below). The slight radial gradient of the CH_4 profile in [Fig. 2](#) exhibiting the maximum at the catalytic surface indicates some desorption of methane molecules from the catalytic surface in that region.

5.4. Impact of flow rate on coke formation on the catalyst

Since oxygen is consumed much faster than the fuel at stoichiometric conditions, the catalyst will experience pyrolysis conditions at some point downstream the catalytic monolith, even though the steam and CO_2 present may prevent coking. In [Fig. 11](#), the computed surface coverages on the Rh catalyst are shown as function of the axial (flow) direction. At lean conditions, $C/O = 0.8$, most of the adsorption sites are vacant, oxygen coverage decreases rather slowly and is still significant at the catalyst exit.

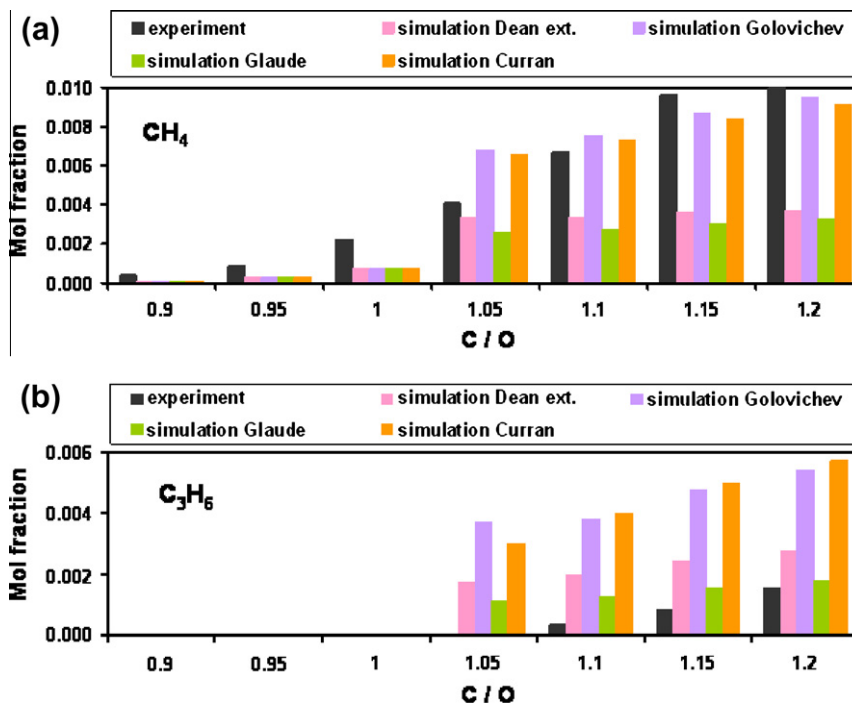


Fig. 10. Numerically predicted and experimentally measured methane (a) and propylene (b) mole fractions as function of C/O ratio at 4 slpm. Simulation of partial oxidation of iso-octane using a one-dimensional flow model and five different gas-phase reaction mechanisms; the C/O dependent catalyst outlet temperature was chosen as constant temperature profile.

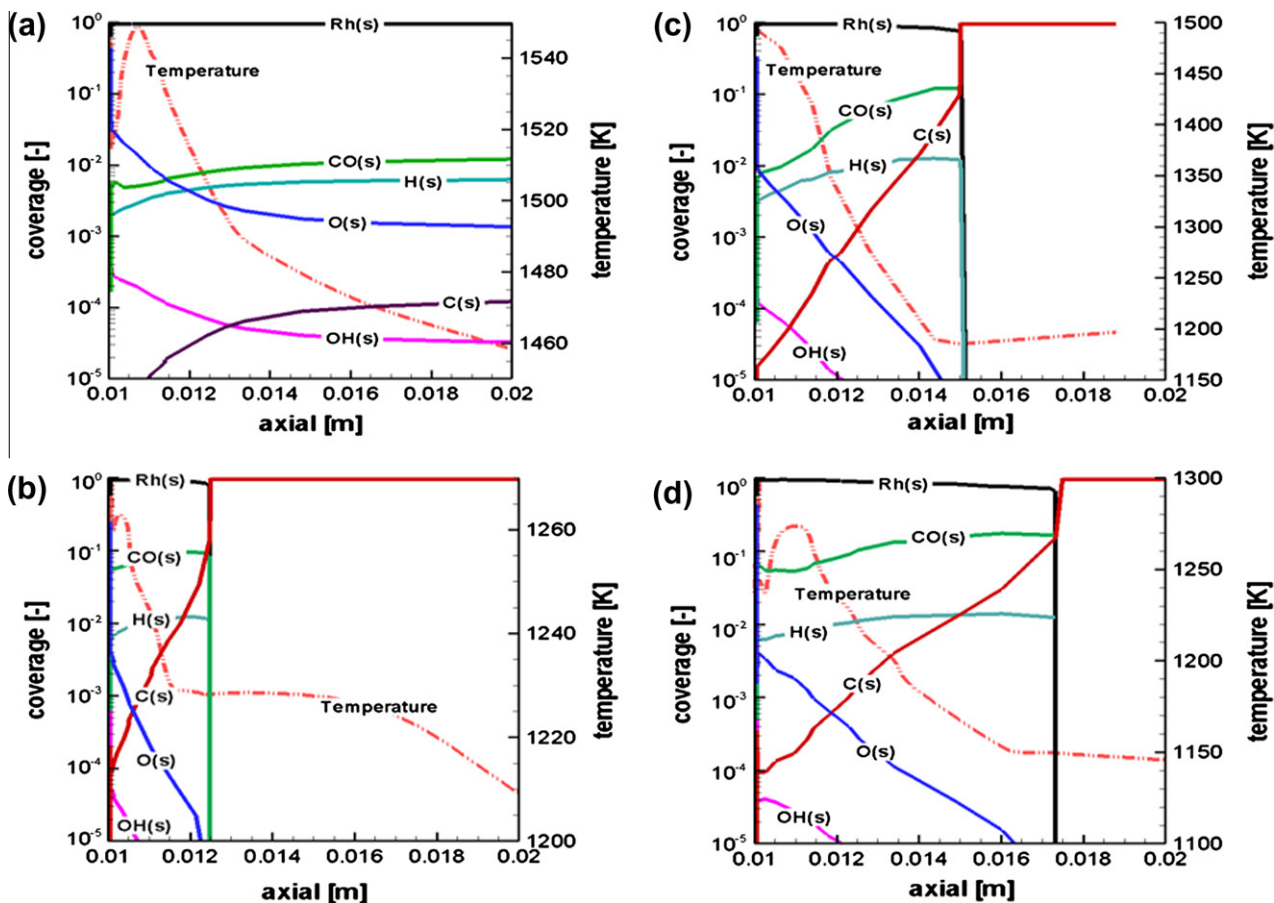


Fig. 11. Numerically predicted surface coverage and surface temperature in a channel in the centerline of the catalytic monolith (a) C/O = 0.8; 5 slpm, (b) C/O = 1.0 and 2 slpm, (c) C/O = 1.0 and 5 slpm, (d) C/O = 1.0 and 6 slpm. Rh(s) denotes vacant adsorption sites.

Carbon atoms cover only a small amount of adsorption sites. The catalyst does not exhibit any coke layer in the experiment.

This picture changes qualitatively with increasing C/O ratio. At C/O = 1.0, the amount of adsorbed oxygen decreases much faster, and is only significant in the entrance region where total oxidation occurs. Carbon atoms, C(s), increasingly cover the Rh catalyst and lead to the formation of a full monolayer of carbon at a certain position downstream the catalyst. This transition point depends on the flow rate, the lower the flow rate, the more upstream this transition point can be observed. The oxidation and reforming reactions are obviously conducted in a decreasing catalyst section with decreasing amount (mass) of reactants. Gas-phase reactions leading to the undesired coke precursors occur primarily downstream this transition point; compare Figs. 7 and 11c. As long as the catalyst sustains a sufficient number of vacant sites it serves as sink for radicals produced in the gas-phase and gas-phase reactions can basically be neglected.

The on-set of coke formation at a certain point in the catalytic monolith has been shown experimentally before [44]. Although the actual axial point at which coke formation starts varies from channel to channel due to slight variations in catalyst loading and inlet mass flow in the technical system, the trends are clear: coke formation moves upstream with increasing C/O and decreasing flow rate. Also radial profiles of the *coking-line* over the entire monolithic catalyst have been seen, because the heat transfer effects discussed above vary the distance at which the gas-phase composition at the catalytic surface reaches the critical point at which coking occurs.

Again, the results point to the existence of an optimum flow rate for operation of the reformer: too small flow rates favor coke formation on the catalyst and subsequently the formation of coke precursors by gas-phase reactions; too high flow rates avoid completion of hydrogen producing reactions (above the 6 slpm for the reactor studied here). The latter one also has the disadvantage of increased downstream coke formation, because the outlet temperature is higher and more fuel remains in the product stream, which is more difficult to be quenched to freeze post-reactions.

6. Conclusions

The implementation of detailed heterogeneous and homogeneous reaction mechanisms in a two-dimensional parabolic flow model for the description of the behavior of individual monolith channels and the coupling with heat balances of the catalytic monolith as well as heat shields, insulation, and reactor wall provides a simulation tool that is able to analyze the behavior of structured CPOX reactors in great detail. The simulation can provide guidance to reactor design and optimization of the operating conditions such as flow rate and fuel/oxygen ratio.

This concept is applied here to better understand the reactor behavior of CPOX reactors used as compact reformers for the production of hydrogen-rich synthesis gas from logistic fuels. Iso-octane is used as gasoline fuel-surrogate and the catalyst of choice here is rhodium impregnated into alumina washed on the inner channel walls of a honeycomb monolith. Foam and honeycomb heat shields are attached to the front and back of the catalyst, respectively, to minimize heat loss. Experimental data of a recently published [55] study on CPOX of iso-octane over Rh at varying flow rate and fuel-to-oxygen ratio is taken as reference for this numerical study. Since the reactor works most efficiently concerning hydrogen yields and prevention of coke precursors at molar C/O ratios between 0.8 and 1.0, this study in particular analyzes the behavior at these two limits.

In general it is found that the major objective of the reactor, i.e. production of high hydrogen yields at minimal formation of coke

precursors, can be achieved at C/O ratios close to 1.0 and sufficiently but not extremely high flow rates. The counter-intuitive increase in fuel conversion with decreasing residence time (increasing flow rate) is explained by analyzing the ratio of chemical heat release to heat loss in the reactor. The front heat shield preheats the inlet flow but to a level only, at which gas-phase reactions are not significant yet. Formation of coke precursors, in particular propylene and subsequently ethylene, and formation of methane, start at a position within the catalytic monolith at which oxygen is already totally consumed. With increasing C/O ratio and decreasing flow rate, the position of the on-set of coke formation on the catalyst moves upstream; at C/O = 0.8 the catalyst does not exhibit any coke layer.

A skeletal (semi-reduced) gas-phase reaction mechanism, which still can be handled in the numerical simulation, can be used for the description of gas-phase chemistry in this CPOX reactor. Actually, the skeletal but also four detailed mechanisms reproduce all experimental trends surprisingly well, taking into account that none of the mechanisms was established for the very rich conditions occurring in this reactor.

In the simulation, the reaction mechanisms were taken from literature without any modification, all physical parameters were either directly taken from the experiment or estimated in accordance to the materials and conditions used in the experiment. Simulation of all flow rates and C/O ratios discussed used exactly the same set of parameters. Hence, the model presented seems reliable enough to be used for optimization of reactor design and operating conditions. For instance, the impact of materials properties such as heat conductivity of the insulation and the heat shields, channel diameter, catalyst loading, and exhaust gas recycling may be pre-analyzed on the computer leading to a minimized number of prototypes needed for the development of an adequate technical device.

The core of this combined model surely is the reaction kinetics, which can only be reliably described by elementary-step based heterogeneous and homogeneous reaction mechanisms. These mechanisms can be semi-reduced, as here, for the homogeneous conversion and they can contain some lumped steps, as here, for the heterogeneous conversion. However, real logistic fuels will add another level of complexity to these mechanisms, because the reactivity of complex fuel mixtures is far away from being a proportional combination of the single components. Nevertheless, choosing adequate surrogates and studying their behavior in detail will support technical realization of compact, autothermal fuel reformers.

Acknowledgments

We thank the Umicore AG (Hanau/Germany) for providing the model catalyst. This study was financially supported by the German Research Foundation (DFG).

Appendix A. Supplementary material

Supplementary data associated with this article can be found, in the online version, at [doi:10.1016/j.combustflame.2010.11.004](https://doi.org/10.1016/j.combustflame.2010.11.004).

References

- [1] J. Warnatz, R.W. Dibble, U. Maas, *Combustion, Physical and Chemical Fundamentals, Modeling and Simulation, Experiments, Pollutant Formation*, Springer-Verlag, New York, 1996.
- [2] D.L. Baulch, C.J. Cobos, R.A. Cox, C. Esser, P. Frank, T. Just, J.A. Kerr, M.J. Pilling, J. Troe, R.W. Walker, J. Warnatz, *J. Phys. Chem. Ref. Data* 21 (1992) 411.
- [3] J.A. Miller, R.J. Kee, C.K. Westbrook, *Annu. Rev. Phys. Chem.* 41 (1990) 345.
- [4] C.K. Westbrook, F.L. Dryer, *Prog. Energy Combust. Sci.* 10 (1984) 1.
- [5] K. Kohse-Hoinghaus, R.S. Barlow, M. Alden, E. Wolfrum, *Proc. Combust. Inst.* 30 (2005) 89.

- [6] R.G. Susnow, A.M. Dean, W.H. Green, P. Peczak, L.J. Broadbelt, J. Phys. Chem. A 101 (1997) 3731.
- [7] R.J. Kee, F.M. Rupley, J.A. Miller, M.E. Coltrin, J.F. Grcar, E. Meeks, H.K. Moffat, A.E. Lutz, G. Dixon-Lewis, M.D. Smooke, J. Warnatz, G.H. Evans, R.S. Larson, R.E. Mitchell, L.R. Petzold, W.C. Reynolds, M. Caracotsios, W.E. Stewart, P. Glarborg, C. Wang, O. Adigun, CHEMKIN, 3.6 ed., Reaction Design, Inc., San Diego, 2000. <www.chemkin.com>.
- [8] R.J. Kee, M.E. Coltrin, P. Glarborg, Chemically Reacting Flow, Wiley-Interscience, 2003.
- [9] B. Hellsing, B. Kasemo, Chem. Phys. Lett. 148 (1988) 465.
- [10] M.E. Coltrin, R.J. Kee, F.M. Rupley, SURFACE CHEMKIN (Version 4.0): A Fortran Package for Analyzing Heterogeneous Chemical Kinetics at a Solid-Surface – Gas-Phase Interface, SAND91-8003B, Sandia National Laboratories, 1991.
- [11] D.A. Hickman, L.D. Schmidt, AIChE J. 39 (1993) 1164.
- [12] J. Warnatz, Proc. Combust. Inst. 24 (1992) 553.
- [13] O. Deutschmann, F. Behrendt, J. Warnatz, Catal. Today 21 (1994) 461.
- [14] W.R. Williams, C.M. Marks, L.D. Schmidt, J. Phys. Chem. 96 (1992) 5922.
- [15] P.A. Bui, D.G. Vlachos, P.R. Westmoreland, Ind. Eng. Chem. Res. 36 (1997) 2558.
- [16] U. Dogwiler, P. Benz, J. Mantzaras, Combust. Flame 116 (1998) 243.
- [17] J. Mantzaras, C. Appel, P. Benz, Proc. Combust. Inst. 28 (2000) 1349.
- [18] R. Carroni, T. Griffin, J. Mantzaras, M. Reinke, Catal. Today 83 (2003) 157.
- [19] D.A. Hickman, L.D. Schmidt, Science 259 (1993) 343.
- [20] M.C. Huff, L.D. Schmidt, J. Catal. 149 (1993) 127.
- [21] K. Maruta, K. Takeda, J. Ahn, K. Borer, L. Sitzki, P.D. Ronney, O. Deutschmann, Proc. Combust. Inst. (2002) 29.
- [22] G. Vesper, Chem. Eng. Sci. 56 (2001) 1265.
- [23] D.K. Zerkle, M.D. Allendorf, M. Wolf, O. Deutschmann, J. Catal. 196 (2000) 18.
- [24] M.C. Huff, I.P. Androulakis, J.H. Sinfelt, S.C. Reyes, J. Catal. 191 (2000) 46.
- [25] D. Chatterjee, O. Deutschmann, J. Warnatz, Faraday Discuss. 119 (2001) 371.
- [26] R.E. Hayes, L.S. Mukadi, M. Votsmeier, J. Gieshoff, Top. Catal. 30–1 (2004) 411.
- [27] S. McIntosh, R.J. Gorte, Chem. Rev. 104 (2004) 4845.
- [28] E.S. Hecht, G.K. Gupta, H.Y. Zhu, A.M. Dean, R.J. Kee, L. Maier, O. Deutschmann, Appl. Catal. A: Gen. 295 (2005) 40.
- [29] J.J. Krummenacher, K.N. West, L.D. Schmidt, J. Catal. 215 (2003) 332.
- [30] J. Thormann, L. Maier, P. Pfeifer, U. Kunz, O. Deutschmann, K. Schubert, Int. J. Hydrogen Energy 34 (2009) 5108.
- [31] A. Lindermeir, S. Kah, S. Kavurucu, M. Muhlner, Appl. Catal. B-Environ. 70 (2007) 488.
- [32] A.D. Qi, S.D. Wang, C.J. Ni, D.Y. Wu, Int. J. Hydrogen Energy 32 (2007) 981.
- [33] B.J. Dreyer, I.C. Lee, J.J. Krummenacher, L.D. Schmidt, Appl. Catal. A: Gen. 307 (2006) 184.
- [34] L. Bobrova, I. Zolotarsky, V. Sadykov, V. Sobyenin, Int. J. Hydrogen Energy 32 (2007) 3698.
- [35] S. Jain, H.Y. Chen, J. Schwank, J. Power Sources 160 (2006) 474.
- [36] L.F. Brown, Int. J. Hydrogen Energy 26 (2001) 381.
- [37] R.P. O'Connor, E.J. Klein, L.D. Schmidt, Catal. Lett. 70 (2000) 99.
- [38] C. Severin, S. Pischinger, J. Ogrzewalla, J. Power Sources 145 (2005) 675.
- [39] O. Deutschmann, L.D. Schmidt, AIChE J. 44 (1998) 2465.
- [40] R. Quiceno, J. Perez-Ramirez, J. Warnatz, O. Deutschmann, Appl. Catal. A: Gen. 303 (2006) 166.
- [41] M. Geske, K. Pelzer, R. Horn, F.C. Jentoft, R. Schlogl, Catal. Today 142 (2009) 61.
- [42] A. Beretta, L. Piovesan, P. Forzatti, J. Catal. 184 (1999) 455.
- [43] A. Beretta, E. Ranzi, P. Forzatti, Chem. Eng. Sci. 56 (2001) 779.
- [44] M. Hartmann, L. Maier, O. Deutschmann, Combust. Flame 157 (2010) 1771.
- [45] R. Schwiedernoch, S. Tischer, C. Correa, O. Deutschmann, Chem. Eng. Sci. 58 (2003) 633.
- [46] D.D. Nogare, N.J. Degenstein, R. Horn, P. Canu, L.D. Schmidt, J. Catal. 258 (2008) 131.
- [47] M. Hartmann, S. Lichtenberg, N. Hebben, D. Zhang, O. Deutschmann, Chem. Ing. Tech. 81 (2009) 909.
- [48] T. Kaltschmitt, L. Maier, O. Deutschmann, Proc. Combust. Inst. (2010) 33, doi:10.1016/j.proci.2010.05.050.
- [49] S.A. Seyed-Reihani, G.S. Jackson, Appl. Catal. A: Gen. 353 (2009) 181.
- [50] A. Beretta, P. Forzatti, Chem. Eng. J. 99 (2004) 219.
- [51] I. Aartun, H.J. Venvik, A. Holmen, P. Pfeifer, O. Gorke, K. Schubert, Catal. Today 110 (2005) 98.
- [52] I. Tavazzi, M. Maestri, A. Beretta, G. Groppi, E. Tronconi, P. Forzatti, AIChE J. 52 (2006) 3234.
- [53] S. Ding, C.N. Wu, Y.H. Cheng, Y. Jin, Y. Cheng, Chem. Eng. Sci. 65 (1989).
- [54] K.A. Williams, R. Horn, L.D. Schmidt, AIChE J. 53 (2007) 2097.
- [55] M. Hartmann, L. Maier, O. Deutschmann, Appl. Catal. A: Gen. (2010), doi:10.1016/j.apcata.2010.08.051.
- [56] M. Hartmann, T. Kaltschmitt, O. Deutschmann, Catal. Today 147 (2009) S204.
- [57] D.C. Rennard, J.S. Kruger, B.C. Michael, L.D. Schmidt, Indus. Eng. Chem. Res. 49 (2010) 8424.
- [58] J.L. Colby, P.J. Dauenhauer, B.C. Michael, A. Bhan, L.D. Schmidt, Green Chem. 12 (2010) 378.
- [59] C.M. Balonek, J.L. Colby, L.D. Schmidt, AIChE J. 56 (2010) 979.
- [60] N. Hebben, C. Diehm, O. Deutschmann, Appl. Catal. A: Gen. (2010), doi:10.1016/j.apcata.2010.08.055.
- [61] S. Tischer, O. Deutschmann, Catal. Today 105 (2005) 407.
- [62] O. Deutschmann, S. Tischer, S. Kleditzsch, V.M. Janardhanan, C. Correa, D. Chatterjee, N. Mladenov, H.D. Minh, 2.2 ed., DETCHEM™ Software Package, 2008. <www.detchem.com>.
- [63] D.R. Lide, CRC Handbook of Chemistry and Physics, 75th ed., CRC Press, Boca Raton, 1994.
- [64] L.L. Raja, R.J. Kee, O. Deutschmann, J. Warnatz, L.D. Schmidt, Catal. Today 59 (2000) 47.
- [65] S. Tischer, C. Correa, O. Deutschmann, Catal. Today 69 (2001) 57.
- [66] O. Deutschmann, in: H.K.G. Ertl, F. Schüth, J. Weitkamp (Eds.), Handbook of Heterogeneous Catalysis, second ed., Wiley-VCH, Weinheim, 2008, p. 1811.
- [67] H.J. Curran, P. Gaffuri, W.J. Pitz, C.K. Westbrook, Combust. Flame 129 (2002) 253.
- [68] P.A. Glaude, V. Conraud, R. Fournet, F. Battin-Leclerc, G.M. Come, G. Scacchi, P. Dagaut, M. Cathonnet, Energy Fuels 16 (2002) 1186.
- [69] Y.-H. Chen, J.Y. Chen, in: 2005 WSS/CI Meeting, Paper YChenWSSF05, 2005. <<http://repositories.cdlib.org/cpl/cm/YChenWSSF05>>.
- [70] V.I. Golovitchev, F. Tao, L. Chomial, in: SAE Paper 1999-01-3552. <<http://www.tfd.chalmers.se/~valeri/MECH.html>>.
- [71] E. Ranzi, T. Faravelli, P. Gaffuri, A. Sogaro, A. D'Anna, A. Ciajolo, Combust. Flame 108 (1997) 24.
- [72] S. Tanaka, F. Ayala, J.C. Keck, Combust. Flame 133 (2003) 467.
- [73] T. Lovas, F. Mauss, C. Hasse, N. Peters, Proc. Combust. Inst. 29 (2002) 1403.
- [74] M.P. Halstead, L.J. Kirsch, C.P. Quinn, Combust. Flame 30 (1977) 45.
- [75] K.M. Walters, A.M. Dean, H.Y. Zhu, R.J. Kee, J. Power Sources 123 (2003) 182.
- [76] H.D. Minh, H.G. Bock, S. Tischer, O. Deutschmann, AIChE J. 54 (2008) 2432.
- [77] H.D. Minh, H.G. Bock, S. Tischer, O. Deutschmann, Computational Science and Its Applications – Iccsa 2008, Pt 1, Proceedings, vol. 5072, 2008, p. 1121.
- [78] Z. Wang, S.J. Shuai, J.X. Wang, G.H. Tian, Fuel 85 (2006) 1831.
- [79] J. Kusaka, Y. Daisho, T. Saito, JSME Int. J. Ser. B-Fluids Therm. Eng. 40 (1997) 432.
- [80] K.L. Hohn, P.M. Witt, M.B. Davis, L.D. Schmidt, Catal. Lett. 54 (1998) 113.